Determination of opening mode stress intensity factor in edge cracked specimen by means of digital shearography

Danial Ghahremani-Moghadam [1,a], Ali Gallehdari [1,b], Saeid Hadidi-Moud [2,c]

[1] Mechanical Engineering Department, Ferdowsi University of Mashhad, Iran

[2] Mechanical Engineering Department, University of Birjand, Iran

[a] d.g.moghadam@gmail.com, [b] ali_ila84@yahoo.com, [c] s.hadidimoud@gmail.com

Keywords: Stress intensity factor, Digital Shearography, Finite Element Analysis

Abstract

In this paper, digital Shearography as a non-destructive technique is deployed to determine the opening mode stress intensity factor in an edge cracked specimen subjected to tensile loading. The optical setup was consisted of two in-plane illumination sources to determine purposed strain variable and consequently to obtain the opening mode stress intensity factor based on the assumptions of linear elastic fracture mechanics (LEFM). The speckle pattern images taken by a CCD camera were recorded and saved on a computer. In order to utilize the advantage of whole field Shearography and minimise the random experimental errors, the least square technique was used to obtain the stress intensity factors. A finite element model of the specific geometry was constructed, and ABAQUS v6.7 commercial software was used to perform the analyses. Comparison of the experimental data with the numerical results proved the credibility and potential of this non-destructive method as a practical measurement technique. The average difference between the results obtained from experiments and those of finite element analyses was nearly 8%.

Introduction

Shearography is an interferometric technique for strain and deformation. It overmatches its predecessor holography in several aspects. Firstly, Shearography is a self-reference technique and requires no additional reference beam, which simplifies the optical setup. It greatly relaxes the vibration isolation requirement that makes it suitable for applications in hostile environment. Secondly, Shearography enables direct measurement of strain, which makes it insensitive to the disturbance of rigid body movement and being appropriate for debonds and crack detection since flaws in material cause strain concentration. Thirdly, Shearography optical setup is simple and it is convenient to pack up a miniature instrument for handy in-situ application. Due to these distinct advantages Shearography is obtaining more and more acceptance in industry as well as in laboratory since its invention. During the last few decades, quit a large amount of research work regarding Shearography has been conducted. The invention of the first working laser by Theodore H. Maiman in 1960 opened a door to coherent optical metrology. Since then, a series of interferometric optical measuring techniques such as holographic interferometry [1], Shearography [2], moire' interferometry [3] and speckle metrology [4] bloomed to enrich the field of experimental mechanics greatly. Shearography, being one of the most widely applied experimental techniques today, was named in 1982 and it has received a great deal of attention on the part of industrial and research centers [5-13]. In the present work Shearography was used for determination of opening mode SIF in an edge cracked specimen which is subjected to tensile load. Furthermore, finite element simulation of the problem is performed and the experimental results are compared with those of the finite element analysis.

Basis of Digital Shearography Technique

Shearography is a distinct optical interference techniques. In other techniques the interference of waves is conducted through collision of a reference light mass with released waves from the body surface, whereas in Shearography the conducted interference is due to shearing of images in a shearing device. The shearing device can be a glass wedge or a Michelson interferometer, Fig.1.

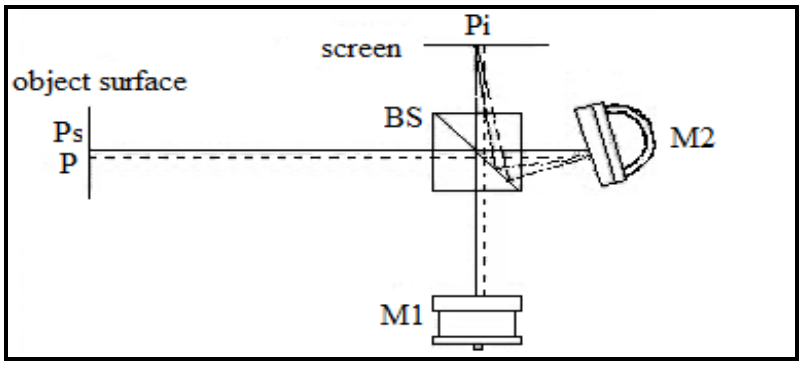

Fig.1. Schematic of waves' interference in Michelson interferometer [3].

As it is obvious in Fig. 1, Michelson interferometer consists of two mirrors M1 and M2 with vertical axes and a laser beam splitter. In this system the released beams from two points P and P_s of body surface interfere with each other at a point P_i on the screen. Also, with rotation of mirror 2 under a small angle a pair of sheared images from object surface are constructed in the camera. Due to interference of the two sheared images a speckle pattern is obtained.

Phase Fringes Pattern Relations

It is clear that by applying a speckle pattern in shearography technique the desired solutions cannot be obtained, so in this technique after applying deformation in object surface, another speckle pattern is provided too and by exerting correlation of two patterns the desired mechanical relations are obtained. To obtain stress intensity factors, two elements of in-plane strain $\frac{\partial u}{\partial x}$ and $\frac{\partial v}{\partial y}$ should be defined by test. To achieve this goal, in this study by using configuration with bi-directional radiation that it is shown in Fig. 2, at any stage of the body status, four images are taken as follows:

1. The first image by making a horizontal shear with size of Δx, source S1 (first light source), axis x as horizontal,
2. The second image by making a horizontal shear with size of Δx, source S2 (second light source), axis x as horizontal,
3. The third image by making a vertical shear with size of Δy, source S1, axis y as horizontal , and
4. The fourth image by making a vertical shear with size of Δy, source S2, axis y as horizontal.

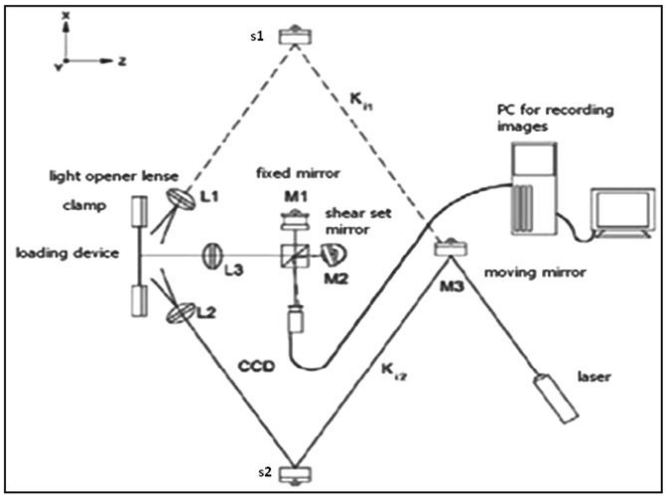

Fig.2. Used digital shearography configuration in test.

It is worth mentioning that axis x is along with width of object and axis y is along with length of object. Now by applying mutual correlation of corresponding images, before and after loading, four phase fringe patterns are obtained.
With a simple subtraction of the phase patterns before and after loading, two desired elements can be obtained as follows:

$$B_1 - B_2 : \Delta\varphi_x = \Delta\varphi_1 - \Delta\varphi_2 = 2K_x \frac{\partial u}{\partial x}\Delta x \tag{1}$$

$$B_3 - B_4 : \Delta\varphi_y = \Delta\varphi_3 - \Delta\varphi_4 = 2K_x \frac{\partial v}{\partial y}\Delta y \tag{2}$$

In above relations, values B correspond with phase fringes pattern in each stage, K_x is radiation wave vector with size of $\frac{2\pi}{\lambda}$ in which laser wavelength λ has been applied. The object rotation has been $\frac{\pi}{2}$ around z axis.
As mentioned before, to obtain phase fringes pattern in each stage a computer program has been written, using MATLAB software environment, algorithm of this program is as follows:
- taking optical intensities images related to two states of object, one before and the other after deformation,
- returning the aforementioned images to RGB environment,
- using a loop by calculation of maximum correlation factor to apply correlation for corresponding similar points of two images,
- obtaining the size and phase of points by applying second Fourier transform, and
- obtaining phase fringes pattern, by subtraction of phase values of two images.

Experimental procedure

The experiment includes nine test cases that were run by three specimens under different load (Table1). To provide sufficient data for the study, six specimens of the same geometry were used as detailed in Fig. 3 and Table 2. To ensure the conditions of uniform tension in the specimens is maintained, the ratio of *L/W* was set to greater than *4*. The specimens were machined out of a 3 mm thick Plexiglas sheet. The Young's modulus and Poisson's ratio of the material were obtained as 3.34 GPa and 0.33, respectively.

Table1. Associated specimen and loading of the test cases

Case	Specimen No.	Loading(N)
1	1	227/6
2	1	433/6
3	1	528/8
4	2	209/9
5	2	334/5
6	2	508/2

The wavelength of the employed He-Ne laser is 632.8(nm). In all test cases the amount of shear was 1mm (in this example $\Delta y = 1mm$). The speckle pattern images taken by the digital camera were recorded and saved on a computer that is shown in Fig. 4. For case 2 subtraction before and after loading images, the fringe demonstration $\frac{\partial u}{\partial x}$ appear. For typical case 2 experimental shearographic fringes is demonstrated in Fig. 5.

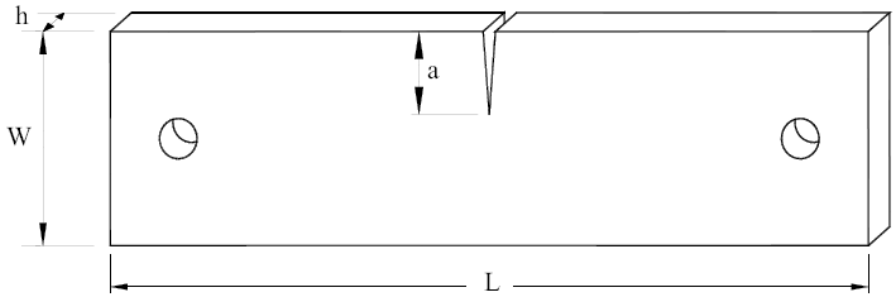

Fig.3. The Scheme of the edge cracked tension specimens

Table1. Geometrical specifications of the edge cracked tension specimens

Specimen no.	Width, W (mm)	Crack length, a (mm)	$\frac{a}{W}$	Thickness, h (mm)	Length, L (mm)
1	55	11	0.2	3	240
2	55	17	0.309	3	240

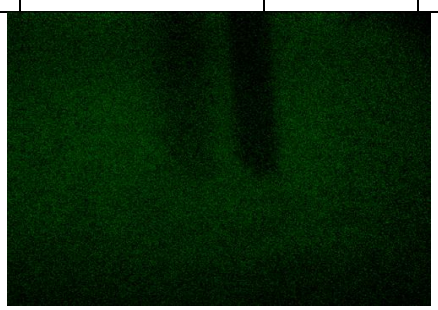

Fig.4. the speckle pattern images taken by the digital camera

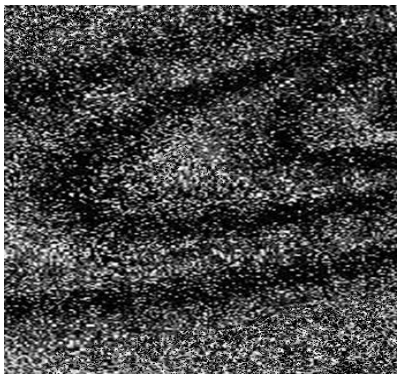

Fig.5. experimental shearographic fringes for typical case 6

Numerical solution

A finite element model of the specific geometry is constructed, and then is analyzed with ABAQUS 6.7. Element CPE4R are used to represent the edge cracked specimen. The plane has modulus of Elasticity of 3.34 (GPa) and Poisson's ratio of 0.33. The tensile force is applied on the specimen. Strain derivative contours at the vicinity of the tip in X direction displayed in Fig. 7. The strain contours at the vicinity of the crack tip is similar to shearographic fringes.

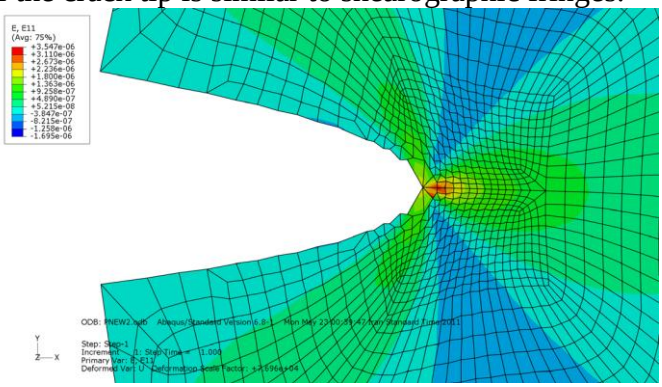

Fig. 7. strain derivative contours at the vicinity of the tip in X direction.

Determination of K_I and K_{II} values using Digital Shearography results

By means of mechanical relation at each point of crack:

$$\sigma_X + \sigma_Y = \sigma_x + \sigma_y \tag{3}$$

And also:

$$\sigma_x + \sigma_y = \frac{E}{1-\nu}(\varepsilon_x + \varepsilon_y) \tag{4}$$

So we have:

$$\sigma_X + \sigma_Y = \frac{E}{1-\nu}(\varepsilon_x + \varepsilon_y) = \frac{E}{1-\nu}\left(\frac{\partial u}{\partial x} + \frac{\partial v}{\partial y}\right) \tag{5}$$

According to relations governing fracture mechanic [14] in the vicinity the tip of crack, σ_x, σ_y for a specimen with a crack which undertakes would be:

$$(\sigma_X)_{\mathrm{I}} = \frac{K_{\mathrm{I}}}{\sqrt{2\pi r}}\cos(\frac{\theta}{2})\left(1-\sin\frac{\theta}{2}\sin\frac{3\theta}{2}\right) \tag{6}$$

$$(\sigma_X)_{\mathrm{II}} = -\frac{K_{\mathrm{II}}}{\sqrt{2\pi r}}\sin(\frac{\theta}{2})\left(2+\cos\frac{\theta}{2}\cos\frac{3\theta}{2}\right) \tag{7}$$

$$(\sigma_Y)_{\mathrm{I}} = \frac{K_{\mathrm{I}}}{\sqrt{2\pi r}}\cos(\frac{\theta}{2})\left(1+\sin\frac{\theta}{2}\sin\frac{3\theta}{2}\right) \tag{8}$$

$$(\sigma_Y)_{\mathrm{II}} = \frac{K_{\mathrm{II}}}{\sqrt{2\pi r}}\cos(\frac{\theta}{2})\sin(\frac{\theta}{2})\cos(\frac{3\theta}{2}) \tag{9}$$

Substituting Eqs (6-9) into Eq (5) in plane strains in the vicinity the tip of the crack would be:

$$\frac{2}{\sqrt{2\pi r}}\left[K_{\mathrm{I}}(\cos(\frac{\theta}{2})) - K_{\mathrm{II}}(\sin(\frac{\theta}{2}))\right] = \frac{E}{1-\nu}(\frac{\partial u}{\partial x}+\frac{\partial v}{\partial y}) \tag{10}$$

Since the illumination angle in -45° as a result we find:

$$\Delta\varphi_x = -\frac{4\pi}{\lambda}\times\frac{\sqrt{2}}{2}\times\frac{\partial u}{\partial x}\times\Delta x \tag{11}$$

And for shearing in y direction considering $\alpha = -45^{\circ}$:

$$\Delta\varphi_y = \frac{4\pi}{\lambda}\times\frac{\sqrt{2}}{2}\times\frac{\partial v}{\partial y}\times\Delta y \tag{12}$$

In plane strains as a function of phase of selected points can be obtained from Eqs (11-12):

$$\frac{\partial u}{\partial x} = -\frac{\Delta\varphi_x}{\frac{2\pi}{\lambda}\cdot\sqrt{2}\cdot\Delta x} \tag{13}$$

$$\frac{\partial v}{\partial y} = \frac{\Delta\varphi_y}{\frac{2\pi}{\lambda}\cdot\sqrt{2}\cdot\Delta y} \tag{14}$$

Substituting Eqs. (13-14) in Eq. (10), the stress intensity factors dependency to phase of points takes the form:

$$\frac{2}{\sqrt{2\pi r}}\left[K_{\mathrm{I}}(\cos(\frac{\theta}{2})) - K_{\mathrm{II}}(\sin(\frac{\theta}{2}))\right] = \frac{E}{(1-\nu)\cdot\frac{2\pi}{\lambda}\cdot\sqrt{2}}(-\frac{\Delta\varphi_x}{\Delta x}+\frac{\Delta\varphi_y}{\Delta y}) \tag{15}$$

Although two data points are sufficient to determine K_{I} and K_{II} but in order to take advantage of whole field shearography and increase the accuracy, the data for several points are registered and least square method is utilized. Then K_{I} and K_{II} are obtained as:

(16)

$$\begin{Bmatrix} K_I \\ K_{II} \end{Bmatrix} = \frac{1}{\left(\frac{2}{\pi}\sum\frac{1}{r_i^2}\cos^2(\frac{\theta_i}{2})\right)\left(\frac{2}{\pi}\sum\frac{1}{r_i^2}\sin^2(\frac{\theta_i}{2})\right)-\left(\frac{1}{\pi}\sum\frac{1}{r_i^2}\sin(\theta_i)\right)^2}$$

$$\begin{bmatrix} \frac{2}{\pi}\sum\frac{1}{r_i^2}\sin^2(\frac{\theta_i}{2})\cdot\frac{E\lambda}{(1-\nu)\cdot2\pi\sqrt{\pi}}\sum(-\frac{(\Delta\varphi)_{xi}}{\Delta x}+\frac{(\Delta\varphi)_{yi}}{\Delta y})\cdot\cos(\frac{\theta_i}{2}) - \frac{1}{\pi}\sum\frac{1}{r_i^2}\sin(\theta_i)\cdot\frac{E\lambda}{(1-\nu)\cdot2\pi\sqrt{\pi}}\sum(-\frac{(\Delta\varphi)_{xi}}{\Delta x}+\frac{(\Delta\varphi)_{yi}}{\Delta y})\cdot\sin(\frac{\theta_i}{2}) \\ -\frac{2}{\pi}\sum\frac{1}{r_i^2}\cos^2(\frac{\theta_i}{2})\cdot\frac{E\lambda}{(1-\nu)\cdot2\pi\sqrt{\pi}}\sum(-\frac{(\Delta\varphi)_{xi}}{\Delta x}+\frac{(\Delta\varphi)_{yi}}{\Delta y})\cdot\sin(\frac{\theta_i}{2}) + \frac{1}{\pi}\sum\frac{1}{r_i^2}\sin(\theta_i)\cdot\frac{E\lambda}{(1-\nu)\cdot2\pi\sqrt{\pi}}\sum(-\frac{(\Delta\varphi)_{xi}}{\Delta x}+\frac{(\Delta\varphi)_{yi}}{\Delta y})\cdot\cos(\frac{\theta_i}{2}) \end{bmatrix}$$

The SIF values are obtained for nine cases as given in Table 3. These SIF values are compared against those obtained through numerical solution.

Table3. Comparison of numerical and digital Shearography SIFs.

Case	$K_{Shearography}(Mpa\sqrt{m})$	$K_{numerical}(Mpa\sqrt{m})$	difference (%)
1	0.315	0.314	0.07
2	0.606	0.598	1.3
3	0.742	0.729	1.7
4	0.426	0.460	8
5	0.694	0.734	5.8
6	1.064	1.115	4.8

Experimental SIF values are compared against those obtained through empirical relations in Table4. For instance, according to [15] the following relations yield first mode SIF for edge cracked specimens with finite dimensions under opening mode loading:

$$K_{\mathrm{I}} = F_{\mathrm{I}}\sigma\sqrt{\pi a} \tag{17}$$

Where,

$$F_{\mathrm{I}} = 1.122 - 0.231(\frac{a}{W}) + 10.55(\frac{a}{W})^2 - 21.71(\frac{a}{W})^3 + 30.382(\frac{a}{W})^4 \tag{18}$$

Table4. Comparison of empirical and digital Shearography SIFs.

Case	$K_{Shearography}(Mpa\sqrt{m})$	$K_{emprical}(Mpa\sqrt{m})$ [7]	difference (%)
1	0.315	0.342	7.9
2	0.606	0.652	7
3	0.742	0.794	6.6
4	0.426	0.464	8.2
5	0.694	0.739	6.1
6	1.064	1.123	5.3

It should be noted that since dark fringes are somewhat thick, the data points are read from centerline of dark fringes. Also the data points too close to the crack tip produce higher errors which must be crossed out. Although as the Table 3,4 indicates the accuracy of the approach, there are some differences due to a few error sources which follows: the distance between crack tip and data points is too small to measure accurately, and locating exact position of the crack tip on images is to some extent troublesome. Furthermore the dark bands of fringes are thick instead of narrow that are due to human eyes which cannot recognize where exactly the light intensity becomes minimum.

Conclusions

In this paper opening mode SIF in cracked specimen has been determined experimentally and numerically. Comparing the experimental and numerical values, the credibility and generality of SIF values are obtained for a cracked specimen by means of non-destructive technique of digital shearography. This comparing shows that the experimental results are reliable. Maximum percentage of the differences was 8.2%, Table 3 shows that for small loads the differences is lower.

References

[1] P.K. Rastogi (ed),Holographic interferometry: principles and methods, Berlin, Springer, (1994).

[2] W. Steinchen and L. X. Yang, Digital Shearography: theory and application of digital speckle pattern shearing interferometry, Bellingham, SPIE Optical Engineering press, (2003).

[3] D. Post, B. Han and P. Ifju, High sensitivity moiré: experimental analysis for mechanics and materials, New York, Springer-Verlag, (1994).

[4] R.S. Sirohi(ed), Speckle metrology, New York, Marcel Dekker, (1993).

[5] Habib, K. "Thermally Induced Deformations Measured by Shearography", J. Optics and Laser Technology, Vol. 37, No. 6, pp. 509-512, (2005).

[6] Santos, F., Vaz, M.M., and Monteiro, J. "A New Set-up for Pulsed Digital Shearography Applied To Defect Detection In Composite Structures", J. Optics and Lasers in Eng. Vol. 42, No. 2, pp. 131-140, (2004).

[7] Kim, K., Kang, K.S., Kang, Y.J., and Cheong, S.K. "Analysis of an Internal Crack of Pressure Pipeline Using ESPI and Shearography", J. Optics & Laser Technology, Vol. 35, No. 8, pp. 639-643, (2003).

[8] Chau, F.S. and Zhou, J. "Direct Measurement of Curvature and Twist of Plates Using Digital Shearography", J. Optics and Lasers in Engineering, Vol. 39, No. 4, pp. 431-440, (2003).

[9] Dilhaire, S., Jorez, S., Cornet, A., Patiño Lopez, L.D., and Claeys, W. "Measurement of the Thermo mechanical Strain of Electronic Devices by Shearography", J. Microelectronics Reliability, Vol. 40, No. 8-10, pp. 1509-1514, (2000).

[10] Steinchen, W., Yang, L.X., Kupfer, G., Mäckel, P., and Vössing, F. "Nondestructive Testing of Aerospace Composite Materials Using Digital Shearography", J. Aerospace Engineering, Vol. 212, No. 1, pp. 21-30, (1998).

[11] Steinchen, W., Yang, L.X., and Kupfer, G. "Digital Shearography for Nondestructive Testing and Vibration Analysis", Experimental Techniques, J. Experimental Mechanics, pp. 20-23, (1997).

[12] Hung, Y.Y. and Long, KW. "Industrial Residual Stress Measurement by Large Shear Computerized Shearography", Proceedings of Industrial Conf. on Advanced Technology in Experimental Mechanics, wakayama, Japan, pp. 406-410, (1997).

[13] Hung, Y.Y. "Application of Digital Shearography for Testing of Composite Structures", J. Composites, Part B 30, pp. 765-773, (1999).

[14] D. Broek, Elementary Eng. Fracture Mechanics, 4th Edition, Kluwer Academic Publisher, Dordrecht, Holland, (1991).

[15] Tada, H., Paris, P.C., and Irwin, G.R. "The Stress Analysis of Cracks Handbook", 3rd Ed., ASME Press, New York, (2000).